Shock Waves (2012) 22:511–519
DOI 10.1007/s00193-012-0382-y

ORIGINAL ARTICLE

Effect of incident shock wave strength on the decay of Richtmyer–Meshkov instability-introduced perturbations in the refracted shock wave

C. Bailie · J. A. McFarland · J. A. Greenough · D. Ranjan

Received: 3 November 2011 / Revised: 9 April 2012 / Accepted: 4 May 2012 / Published online: 14 June 2012

Abstract The effect of incident shock wave strength on the decay of interface introduced perturbations in the refracted shock wave was studied by performing 20 different simulations with varying incident shock wave Mach numbers ($M \sim 1.1-3.5$). The analysis showed that the amplitude decay can be represented as a power law model shown in Eq. 7, where A is the average amplitude of perturbations (cm), B is the base constant ($\text{cm}^{-(E-1)}$), S is the distance travelled by the refracted shockwave (cm), and E is the power constant. The proposed model fits the data well for low incident Mach numbers, while at higher mach numbers the presence of large and irregular late time oscillations of the perturbation amplitude makes it hard for the power law to fit as effectively. When the coefficients from the power law decay model are plotted versus Mach number, a distinct transition region can be seen. This region is likely to result from the transition of the post-shock heavy gas velocity from subsonic to supersonic range in the lab frame. This region separates the data into a high and low Mach number region. Correlations for the power law coefficients to the incident shock Mach number are reported for the high and low Mach number regions. It is shown that perturbations in the refracted shock wave persist even at late times for high incident Mach numbers.

Keywords Richtmyer–Meshkov instability · Shock wave refraction · Shock wave perturbation · Shock tube

Communicated by R. Bonazza.

C. Bailie · J. A. McFarland · D. Ranjan (✉)
Department of Mechanical Engineering, Texas A&M University, 3123 TAMU, College Station, TX 77843, USA
e-mail: dranjan@tamu.edu

J. A. Greenough
Lawrence Livermore National Laboratory, 7000 East Ave., L-95, PO Box 808, Livermore, CA 94550, USA

1 Introduction

Shock waves are fluid mechanics phenomena that occur in many different engineering and scientific applications. They can be characterized by a nearly discontinuous jump in the thermodynamic properties (pressure, temperature, density) between the leading and trailing edges of the wave. The interaction of a shock wave with an interface between two gases is a very complicated problem which has been studied widely since it was first examined in 1960 [1]. At a fluid interface the diffusion layer between different gases or liquids creates a density gradient. When the shock wave interacts with the perturbed fluid interface, vorticity is deposited on the interface due to the misalignment of the pressure and density gradients. This can be seen in the vorticity equation (Eq. 1) in the baroclinic term, where $\nabla\rho$ is the gradient of density and ∇p is the gradient of pressure, $\boldsymbol{\omega}$ is the vorticity, $D\boldsymbol{\omega}/Dt$ is the substantial derivative of $\boldsymbol{\omega}$, u is the velocity, and ν is the kinematic viscosity. The misalignment of the pressure and density gradients is necessary for instability and can stem from perturbations in the fluid interface or in the shock front.

$$D\boldsymbol{\omega}/Dt = \boldsymbol{\omega}\cdot\nabla\boldsymbol{u} + \nu\nabla^2\boldsymbol{\omega}\underbrace{\left[\frac{1}{\rho^2}\nabla\rho\times\nabla p\right]}_{\text{Baroclinic term}} \tag{1}$$

The hydrodynamic instability created from this misalignment of the pressure and density gradients was studied first analytically by Richtmyer [1] and then experimentally by Meshkov [2] and is termed the Richtmyer–Meshkov instability (RMI). The vorticity deposited by the shock wave will lead to stretching of the fluid interface, and thus cause the two fluids to mix and diffuse at an increased rate. The strength of the density gradients will affect the rate of mixing that is created by the RMI. The Atwood number (A) is used as a

measure of the density contrast between the two fluids and is defined in Eq. 2, where ρ_h and ρ_l are the densities of the heavy and light fluids, respectively. The Atwood number tends to 1 for fluids with very different densities and to 0 for fluids that have very similar densities.

$$A = (\rho_h - \rho_l)/(\rho_h + \rho_l) \quad \text{For the light–heavy case.} \qquad (2)$$

The RMI is fundamentally important in many applications including supersonic combustion and astrophysics, [3,4] but the area where it is currently receiving the highest attention is in inertial confinement fusion (ICF). In the case of ICF, the RMI along with the Rayleigh–Taylor instability (RTI) cause turbulent mixing of the high density fuel with low density surrounding material leading to a reduction in the fusion yield [5]. Accurate modeling of the RMI is vital in controlling mixing and improving the performance of ICF. Summaries of the RMI are presented by Brouillette [3] and Zabusky [6].

Experiments on the RMI have been performed for various types of interface perturbations including an oscillating sinusoidal interface [7–9], a bubble interface [10–12], a gas curtain interface [13,14], and a thin membrane separated interface [2,15]. Numerical and analytical work has been performed to describe the growth rate of characteristic formations in the RMI known as spikes and bubbles [16,17]. The behavior of the RMI at higher Mach numbers [11,18], multimode interfaces [19,20], and after the passage of the shock-wave reflected off the end wall through the interface, called re-shock [21,22], have been studied. In addition, computational simulations of the RMI using several different codes [23–25] have allowed the researchers to gain a greater knowledge and understanding of the physics underlying compressible flow while reducing the cost of experimentation.

In the case of RMI, the initial perturbations on the gaseous interface also produce imprints of the perturbations on the shock wave itself. The behavior and decay of perturbations on the refracted shock wave pose many interesting questions to be studied, but these perturbations have received limited attention in published works so far. One study that did examine the perturbations introduced on the refracted shock wave was that of Aleshin et al. [26]. Extended details of this work were presented by Aleshin et al. [27] in a technical report. The authors performed experiments in which a shock wave interacted with a single mode sine wave perturbation created on an interface using a thin film. The purpose of the experiments was to explore how the transmitted shock would be perturbed by this interface perturbation and how the transmitted shock wave perturbation would evolve over time and space. In these experiments the Atwood number and the amplitude to wavelength ratio effects were explored. Schlieren images were used to make measurements of the transmitted shock wave location. While this was the best experimental technique available at the time, the resolution

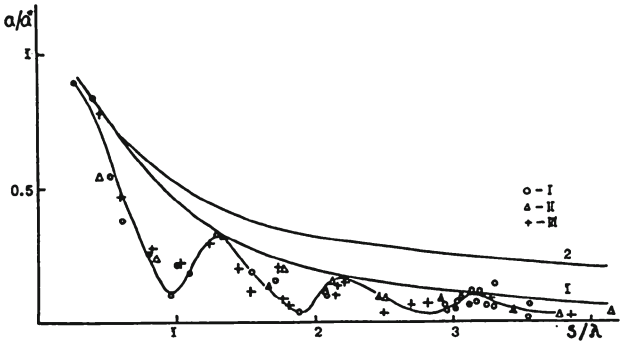

Fig. 1 Damping of perturbations on the shock front: reproduced from Aleshin et al. [26]. Transmitted shock Mach number in experiments is 4, *line 1* is the power law fit for a helium over Xenon interface where symbols *I*, *II*, and *III* in the legend correspond to experimental data for wavelengths of 7.2, 3.6, and 2.4 cm, respectively, *line 2* is the power law fit for Argon over Xenon

of the measurements was severely limited and the measurements were subject to some human interpretation.

The evolution of the transmitted shock wave perturbation was found to be of the form shown in Eq. 3, where a is the amplitude (amplitude will be defined as half the peak to peak amplitude in this paper) of the perturbation, C is a constant, S is the distance travelled by the refracted shockwave, λ is the interface perturbation wave length, and n is the decay constant. Equation 4 gives the predicted initial amplitude of the refracted shock wave perturbation a^*, where a_0 is the initial interface sine wave perturbation amplitude, and w_i and w_t are incident and refracted shock wave speeds. Figure 1 shows the experimental data with the regression fitting the local oscillation peaks. In this study the Atwood number of the interface was varied to find a relationship for n.

$$a/a^* = C(S/\lambda)^n, \qquad (3)$$

$$a^* = a_0(1 - w_i/w_t). \qquad (4)$$

The current work seeks to extend the previous work on refracted shock wave perturbations and the RMI discussed above by exploring the effect of incident shock wave Mach number. The evolution of perturbations introduced by the since wave interface on the transmitted shock wave has seldom been reported in the literature. The decay rate of these perturbations is important for multilayer fluid systems, such as those found in many ICF fuel capsule designs, in which the perturbed shock will interact with additional density gradients. In systems such as these, density gradient perturbations in one layer will cause pressure gradient perturbations which will complicate the RMI generated in subsequent density gradients.

The effect of incident shock wave strength on the decay of interface introduced perturbations in the refracted shock wave was studied in this paper for the first time using simulations. Simulations were performed using the ARES

hydrodynamics code, described in Sect. 2. Twenty incident Mach numbers ranging from 1.1 to 3.5 were studied in simulations which required approximately 20,000 cpu hours each. In the previous experimental work the incident shock wave Mach number was not independently varied and its effect was not explored. The detail provided by these simulations allows features of the flow field not visible in the previous experimental work to be examined. Results for the refracted shock wave perturbation amplitude as a function of distance and initial Mach number are reported below. The emphasis of this paper rests in developing a model to describe the decay of these perturbations and determine what relation, if any, exists between incident Mach number and the decay rate of these perturbations.

2 Computational method

The present study was performed using a staggered mesh arbitrary Lagrange Eulerian (ALE) hydrodynamics code, named ARES, which is under active development at Lawrence Livermore National Laboratory (LLNL). The ARES code is described in detail by McFarland et al. [25]. The Lagrange time advancement is second-order-corrector and uses the Gauss Divergence theorem to give the discrete finite difference equations [25,28]. All numerical differences are fully second order in space. Velocities are defined at mesh nodes while internal energy and density are defined at the zone centers using piecewise constant profiles. Artificial viscosity is used to suppress spurious oscillations [28]. A second-order remap [29] to the Eulerian mesh is applied after the Lagrange step.

All interfaces were treated as miscible numerically, but a diffusion model was not applied. This allowed the initial interface to be diffuse but did not allow for additional diffusion to take place as the interface evolved which would have little effect on the transmitted shock front. Artificial viscosity was applied but boundary layers were not included in the simulation. The boundary conditions of the simulation domain were constructed such that the right wall (downstream) was a reflective boundary in the streamwise direction, and the top and bottom walls were reflecting slip walls with no viscous boundary layer (Fig. 2). The left wall (upstream) contained an inflow source in the streamwise direction at post shock conditions which sustained the incident shock wave. When the interface reflected shock wave intersected the upstream boundary it would reflect as a non-physical expansion wave which would reintersect the refracted shock wave at a later time. This time was well beyond the simulation time over which data was taken and so this non-physical expansion wave had no effect on the results.

The test domain was chosen to measure 250 cm long with a height that varied for each simulation set. The initial location

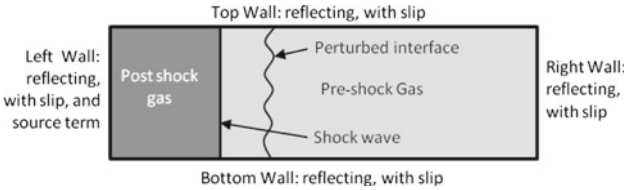

Fig. 2 Schematic of simulation boundary conditions

of the shock wave, and interface as well as the initial interface diffusion thickness and perturbation were set uniquely for the different simulations described below. The resolution for the different simulation sets was chosen so that the number of nodes was constant for the different computational domain sizes used. This resolution was selected on the basis of previous work [25] which incorporates a detailed resolution study. For all simulations the initial temperature and pressure were chosen as 298 K and 0.5 atm, respectively, to match the experimental conditions of Aleshin et al. [26]. A simulation of an experiment performed by Aleshin et al. is presented below for comparison and validation.

3 Simulation of experimental work

To begin the computational work, experimental results from Aleshin et al. [27] for helium over xenon interface with an incident shock wave with Mach number of 2.89 were compared to a two-dimensional ARES simulation under the same initial conditions. The simulation domain had a height of 7.2 cm which corresponded to the shock tube cross section used in the experiments. The interface perturbation was a single mode sine wave with wave number of approximately 1.75 cm^{-1} and amplitude of 2 cm, where the wave number, k, is defined in Eq. 5. The initial conditions of the experiment 633B are summarized in Table 1. The resolution for this simulation was set to 72 μm. The interface and shock wave were initialized at 20 and 10 cm from the left wall, respectively, and the initial interface diffusion thickness was set to 0.2 mm. The experiments used a thin film to separate the gases and this diffusion thickness was chosen to attempt to approximate the diffusion that would take place through the thin film

$$k = 2\pi/\lambda. \tag{5}$$

Table 1 Initial conditions of Aleshin experiment 633B

Initial Mach number	2.89
Gas pair	He–Xe
Atwood number (A)	~0.94
Interface wavelength (λ)	3.6 cm
Interface amplitude (a)	2 cm
Channel height	7.2 cm

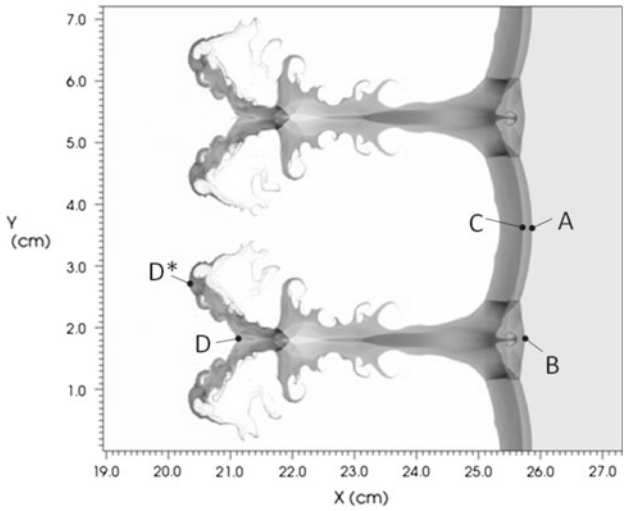

Fig. 3 Density plot showing the location of characteristic points defined by Aleshin et al. in the experimental work

Aleshin et al. measured the velocity of four characteristic points in the system as shown in Fig. 3. *C* is the tip of a bubble, *D* is the end of a spike, *B* is the point on the shock wave at the same vertical location as the tip of a spike, and *A* is the point on the shockwave at the same vertical location as the tip of the bubble. The simulation showed a flow field not just dominated by a single characteristic spike structure, but by a spike which had a 2 point forked tip. D^* was measured as a second possible location of the end of the spike. It is difficult to determine if this forked tip was produced in the experiments, due to the low resolution imagining techniques available at the time. It appears that in some experiments that the forked tip developed while in others it did not. The simulation was carried out to 186 μs where the interface had sufficiently evolved to compare it to the experimental results.

The results of the simulation can be seen in Table 2. The uncertainty in measurement of experiment 633B is ±5 %. Characteristic points *A* and *C* fall within the experimental uncertainty while points *B* and *D* do not. Point *D* was affected by the diverging spike tip, which caused it to slow.

Table 2 Table of velocity measurements taken from Aleshin et al. [27] experiment 633B and derived from ARES simulation of experiment 633B

Aleshin et al.		ARES		Relative error (%)
V_A	0.865	V_A	0.85	1.73
V_B	0.945	V_B	0.891	5.71
V_C	0.65	V_C	0.634	2.46
V_D	0.406	V_D	0.452	11.33
		V_{D^*}	0.367	9.61

Units are cm/μs

The placement of point *D* by ARES did not agree with the experiments; and the comparison of the velocities of points *D* and D^* in ARES to the velocity of experimental data point *D* shows a higher error.

Because the behavior of point *D* is inconsequential to the study of the perturbations on the refracted shock wave, and it is unclear if it was produced in experiments, the ARES simulations were used to predict the behavior of additional experimental parameter sets not explored in the experiments of Aleshin et al. One possible explanation for the difference in the ARES simulations and the experiments is that the simulations were performed in 2D. As the interface evolves beyond the linear regime, traditionally defined as $a/\lambda \ll 1$, three-dimensional effects become increasing important to accurate modeling of the flow.

4 Incident shock wave strength study

4.1 Simulation initial conditions

The effect of incident shock wave strength on the decay of interface introduced perturbations in the refracted shock wave was studied by performing multiple simulations with varying incident shock wave Mach numbers. The interfacial perturbation was sinusoidal in shape with wave number $\sim 0.94\ \mathrm{cm}^{-1}$ centered vertically in the channel 30 cm from the left boundary (Fig. 4). The amplitude of the wave was 2.5 cm. The initial diffusion thickness in the mixing layer was set to 1 mm to simulate a membrane-less experiment. The shock wave was initialized at 10 cm from the left boundary. For this Mach number study, the gas pair was chosen to be Air-SF_6, as many of the RMI studies in the past have been carried out for this specific gas pair. In these simulations the molecular weight of air and SF_6 is taken to be 30 and 146 g/mol, respectively. The specific heat ratio (gamma) for air and $SF_6$is set to 1.4 and 1.09, respectively. The spatial resolution in the simulation was 100 μm, using a mesh with unity aspect ratio. This gives 1,000 zones across the 10 cm channel. The initial conditions of the incident shock wave strength study are summarized in Table 3. The initial Mach number in the study was varied between 1.1 and 3. 5 (Table 4).

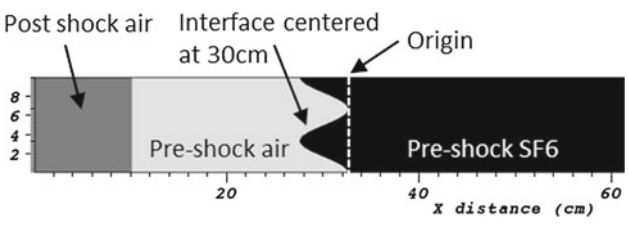

Fig. 4 Density plot of initial conditions for all Mach numbers

Table 3 Initial conditions of shock strength study

Gas pair	Air-SF6
Atwood number (A)	~0.67
Interface wavelength (λ)	~6.67 cm
Interface amplitude (a)	2.5 cm
Channel height	10 cm

4.2 Data processing

In order to evaluate the decay of perturbations in the refracted shock wave, the position of the shock wave, and amplitude of the perturbations in it need to be tracked throughout the simulation. For each case, the leading edge of the shockwave was isolated at every time step as a series of discrete spatial points using the data visualization and analysis software package, VisIt. The average of the horizontal coordinates of the points was taken to be the mean location of the refracted shockwave at a given time step. The amplitude of the perturbation can be expressed as the sum of the absolute values of the deviation at every point of the shock wave location, as seen in Eq. 6, where n is the number of points on the leading edge of the shock wave, X_i is the horizontal coordinate of the nth point, and $\bar{X}$ is the mean location of the shockwave.

$$\frac{1}{n}\sum_{1}^{n}|\bar{x}-x_i|. \tag{6}$$

The location of the shock wave was then plotted as the distance it had travelled from its origin, the mean location of the initial interface (30 cm). Graphs of the perturbation amplitude as a function of the mean shock wave location were constructed, as seen in Fig. 5. The fluctuating nature of the perturbation amplitude is due to the reverberating shock waves which traverse the flow field and are normal to the refracted shock wave (Fig. 6). These fluctuations form local maxima points shown in Fig. 5.

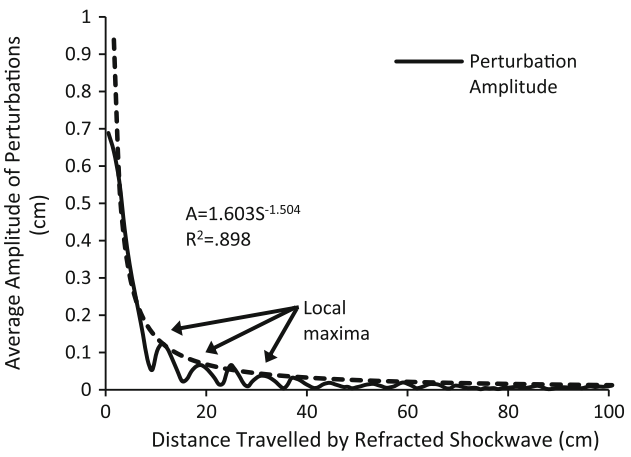

Fig. 5 Average amplitude of perturbations versus distance travelled by refracted shockwave for Mach 1.5 with power law regression shown as *dashed line*

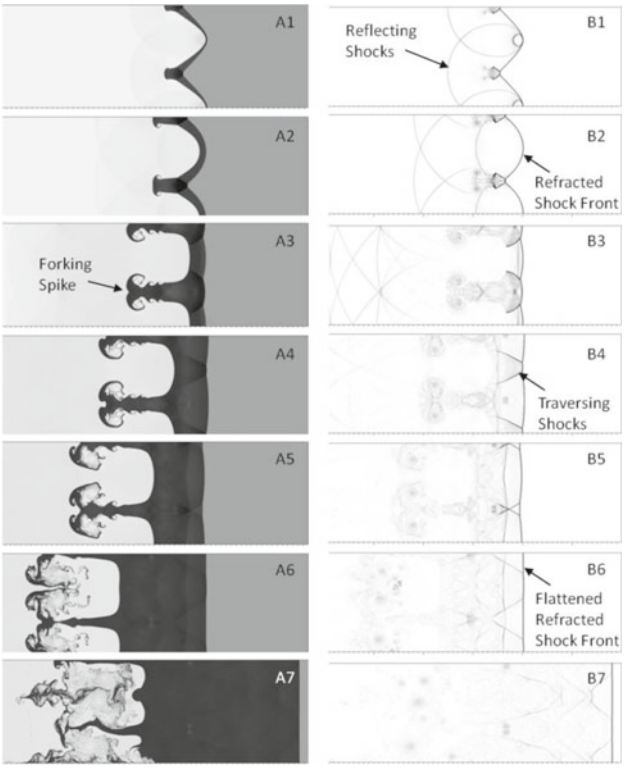

Fig. 6 Times series of plots for incident shock wave Mach number of 1.5. Series *A* shows density plots. Series *B* shows pressure gradient plots. Images *1–7* are for refracted shock front travelled distances of 1.75, 3.75, 8.75, 13.75, 18.75, 28.75, 48.75 cm, respectively

Figure 6 shows a time series of density and pressure gradient plots taken for various distances travelled by the refracted shock front. These plots illustrate the flow field structures which affect the perturbation amplitude. The traversing shock waves are clear in Fig. 6-B4. In Fig. 6-B6 it can be seen that the refracted shock front has nearly replanarized at a travelled distance of 28.75 cm. The density plots show similar flow features discussed in the previous section for reproduction of Aleshin et al. experiments. It should be noted that the forking in the spike tip is clearly visible in this case also. This has been highlighted in Fig. 6-A3.

Extensive non-linear regression analysis was performed on the entire data set. The analysis showed that the amplitude decay can be represented as a power law model shown in Eq. 7, where A is the average amplitude of perturbations (cm), B is the base constant ($\mathrm{cm}^{-(E-1)}$), S is the distance travelled by the refracted shockwave (cm), and E is the power constant. It should be noted that while this is the same form as that proposed by Aleshin et al. [26,27] and reported on in Sect. 1, a dimensional form of the equation was used here instead since Atwood number and amplitude to wavelength ratios were not explored, and the curve fit was applied to the entire

data set instead of just the peak locations. These modifications to the methods of the previous work resulted in a better defined curve fit with less human interpretation required. The choice of the power law decay model was purely empirical in that it provided the best fit to data. Data points were taken starting at the moment the incident shock had fully refracted into the SF_6. The average horizontal location of the shock front at this moment varied for different incident Mach numbers. This location was estimated as 31.25 cm with an error of below 1 % for all incident shock Mach numbers. It should be noted that the data start location can have a large effect on the power law coefficients for low Mach numbers. The coefficients for the power law regression of the Mach 1.5 data set is shown in Fig. 5 with its associated coefficient of determination (R^2) value. The R^2 value and its interpretation will be discussed in the next section.

$$A = B * S^E, \tag{7}$$

4.3 Results and discussion

Simulations were carried out for 20 different incident shockwave Mach numbers from 1.1 to 3.5. The data was processed to find the coefficients for a power law regression of the perturbation amplitudes as discussed above in Sect. 4.2. Table 4 lists the power law constants for each case according to Eq. 7 and the R^2 values.

Figure 7 shows the R^2 values of the power regression over the range of Mach numbers, where R^2 is one minus the ratio of the variance of the model error to the variance of the data, and shows how well the regression predicts the behavior of the data. Equation 8 defines R^2, where Y_i is the data point, $\bar{Y}$ is the average of the data, and f_i is the value predicted by the regression equation. The primary contribution to the degradation of the R^2 value comes from the oscillatory nature

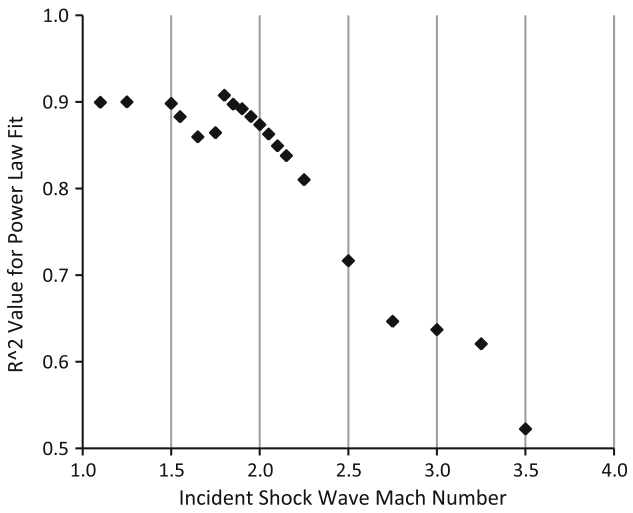

Fig. 7 R^2 values of power regression for each Mach number case

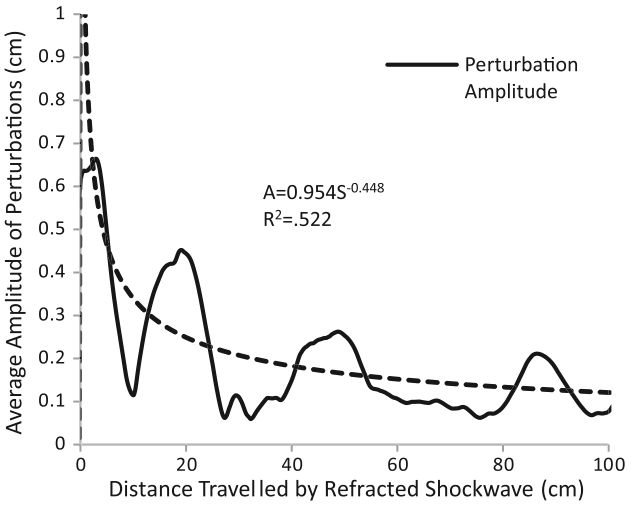

Fig. 8 Average amplitude of perturbations versus distance travelled by refracted shockwave for Mach 3.5 with power law regression shown as *dashed line*

Table 4 List of power law constants derived by power law regression for each Mach number case

Mach	B	E	R^2
1.100	1.631	−1.094	0.900
1.250	1.635	−1.099	0.900
1.500	1.603	−1.054	0.898
1.550	1.504	−1.015	0.883
1.650	1.312	−0.953	0.860
1.750	1.502	−1.003	0.864
1.800	2.095	−1.135	0.908
1.850	1.948	−1.098	0.897
1.900	1.764	−1.033	0.892
1.950	1.602	−0.968	0.883
2.000	1.419	−0.881	0.874
2.050	1.362	−0.840	0.863
2.100	1.246	−0.776	0.849
2.150	1.179	−0.738	0.838
2.250	1.210	−0.721	0.810
2.500	1.279	−0.653	0.717
2.750	1.183	−0.602	0.647
3.000	1.056	−0.533	0.637
3.250	1.080	−0.517	0.621
3.500	0.954	−0.448	0.522

of the data sets which produces an increased variance of the model error. For high Mach numbers at late times the oscillations become large, with larger periods (Fig. 8). As shown in Table 4, these high Mach number sets produce lower R^2 values (0.52 at Mach 3.5). Considering the large variance in the high Mach number data sets where the R^2 value drops, and the oscillatory nature of the data, it is believed the power

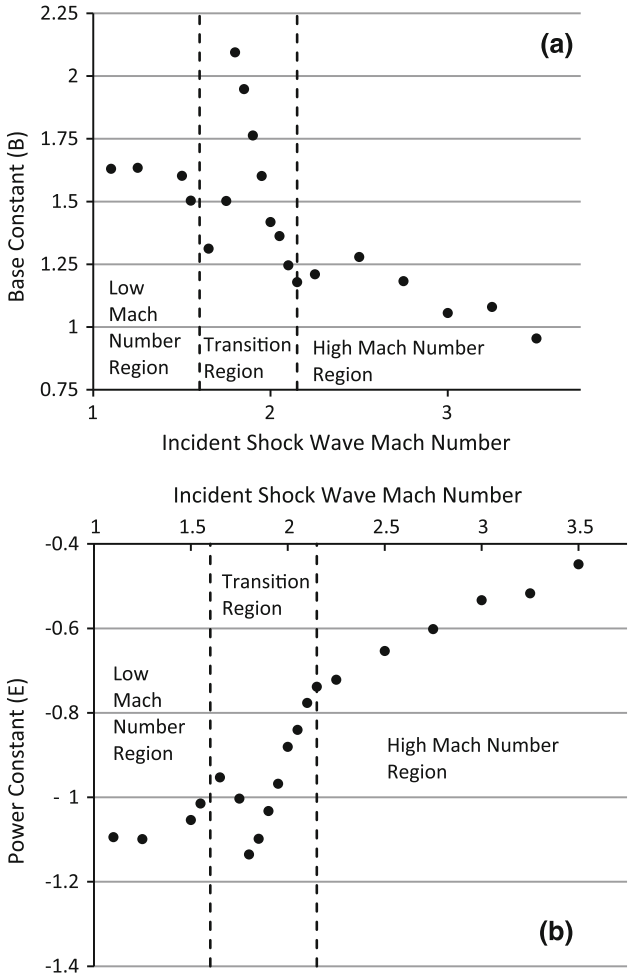

Fig. 9 **a** Base constant of power regression versus Mach number. **b** Power constant of power regression versus Mach number

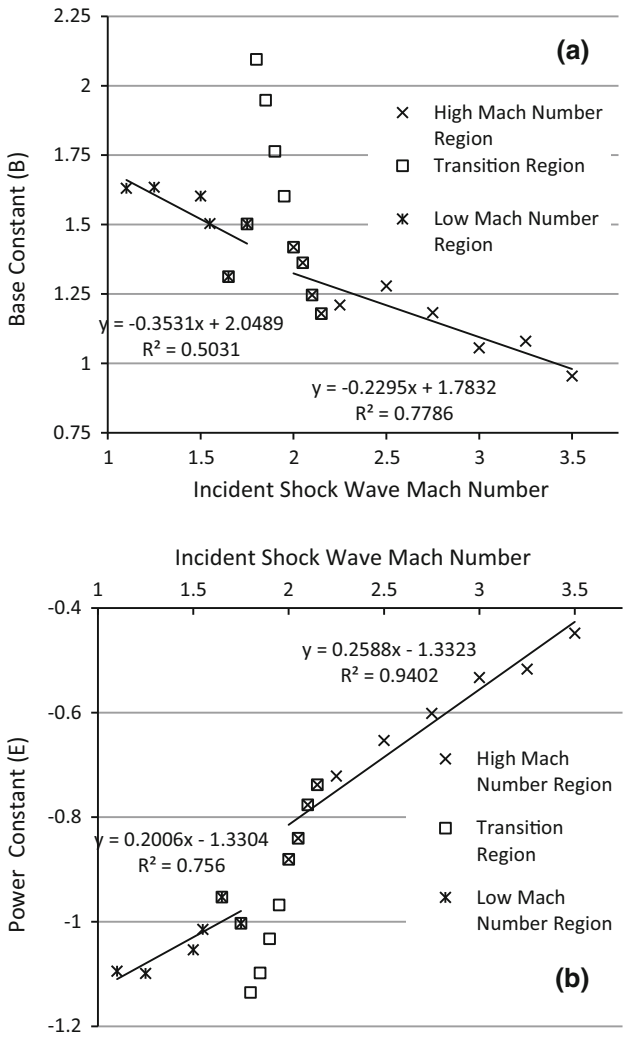

Fig. 10 **a** Base constant versus Mach number. **b** Power constant versus Mach number. Low Mach numbers follow a linear trend between Mach 1.1 and 1.75. High Mach numbers follow a linear trend between Mach 2 and 3.5

law regression is adequate for describing the behavior of the decay.

$$R^2 = 1 - \sum (Y_i - f_i)^2 \Big/ \sum (Y_i - \bar{Y})^2 \,. \tag{8}$$

When the base and power constants are plotted against Mach number (Fig. 9), a clear transition region can be seen between approximately Mach 1.75 and 2. This transition region seems to divide the data into two regions with separate correlations, one for high incident Mach number, and another for low incident Mach number. This transition region is caused by a resonance in the secondary shock waves that traverse the primary shock front. This resonance seems to peak at an incident mach number of 1.85.

As seen in Fig. 9a, the base constant trends downward before turning less steeply downward after the transition region. In Fig. 9b, the power constant trends upward before the transition region and then resumes its upward trend at a slightly increased slope after the transition region.

Figure 10a shows the trends of the base constant in the two Mach regions. The linear trend is nearly continuous through the transition region if the transition data points are neglected. The base constant is related to the post shock interface amplitude since the peaks of the oscillating perturbation amplitude are scaled by the base constant. As the incident shock strength increases the post shock interface amplitude decreases as does the base constant. Theoretically, this means the base constant should be a simple function of the post shock amplitude but in practice it is complicated at late times by interactions with the decay rate of the perturbations.

In Fig. 10b, the trend of the power constant at low and high Mach numbers can be seen to be linear like the base constant. If the transition region data are ignored again the power constant data can be seen to also have a nearly continuous linear trend. The power constant is driven by decay of

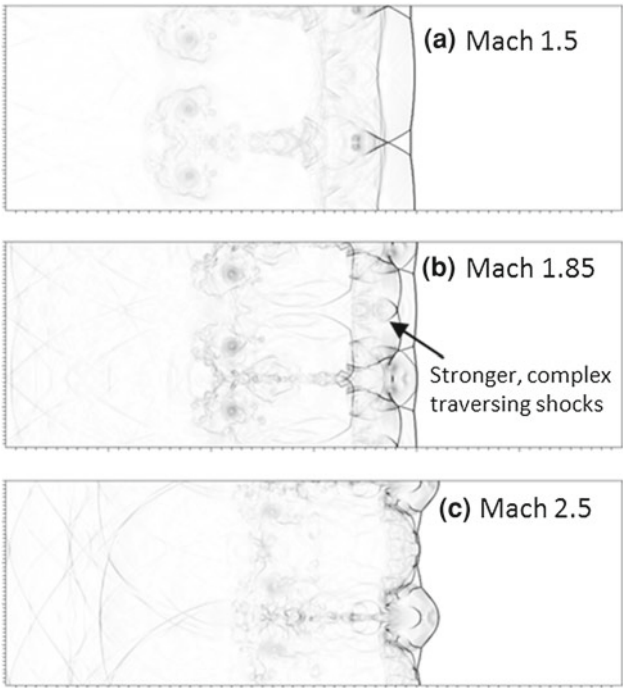

Fig. 11 Gradient of pressure plots for 3 Mach numbers. **a** Mach 1.5, **b** Mach 1.85, **c** Mach 2.5, at a refracted shock travelled distance of 28.75 cm

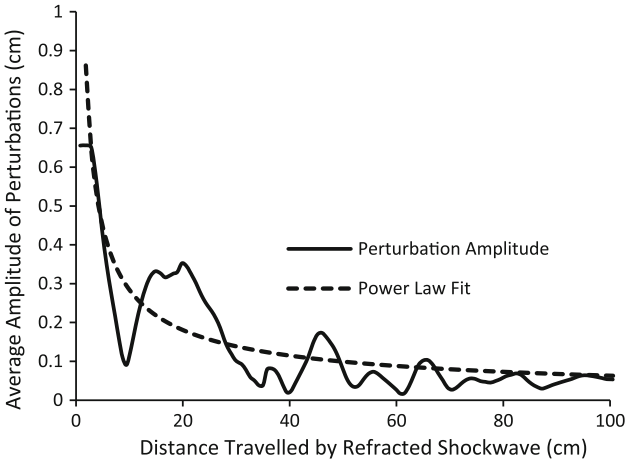

Fig. 12 Average amplitude of perturbations versus distance travelled by refracted shockwave with local maxima shown as *dots* and a power law regression of local maxima as *dashed line* for an incident shock Mach number of 2.5

the perturbation waves as they interact with each other. The high Mach number perturbation waves possess more energy and are able to persist through more wave interactions allowing them to remain stronger at greater distances downstream from the initial interface location. This is why the power constant increases with incident shock strength.

The existence of the transition region may be due to the complexities of the transition to a supersonic post-shock flow and the increasingly coupled flow caused by it. These secondary shock waves may complement or interfere with the refracted shock wave amplitude depending on the phase of the perturbations on the refracted shock wave. This kind of interaction can cause the resonance observed in the Mach 1.85 shock wave flow field. Figure 11 shows the complexity and strength of these secondary waves is much higher for the Mach 1.85 case where resonance occurs. According to 1D gas dynamics this transition should occur near an incident Mach number of 1.5, but for a 2D flow this transition Mach number is less definite and can occur at higher Mach numbers.

At low Mach numbers the constants act to create a fast decay in the perturbation of the refracted shock with small amplitude perturbation remaining to late times (Fig. 10). The low Mach number cases correspond to large (more negative) power constants and larger base constants. The large power constants cause a faster decay and the large base constants result in small amplitudes lingering at late times.

In the high Mach number regime, the decay is characterized by small power constants and smaller base constants. Small power constants cause slow decay (Fig. 10). By this token, the effect of perturbing the shock wave by the density interface is more significant at late times for high Mach number cases. For example, in the simulation for incident Mach number of 1.5 (Fig. 5), the average amplitude of perturbations at approximately 1.0 m from the initial location of the refracted shockwave was ~0.01 cm, whereas for Mach 2.5 (Fig. 12) the amplitude was ~0.07 cm. This amplitude is ~10 % of the initial refracted shock wave amplitude, and is ~3 % of the initial interface perturbation, which may be large enough to create noticeable effects in the baroclinic vorticity production if it intersects a second interface or returns as a reshock.

5 Conclusions

The results presented here show that the power law decay method, similar to the one proposed by Aleshin et al. [26], can be used to describe the decay of the perturbations present on the shock wave created when it encounters a perturbed variable density interface. The proposed model fits the data for low incident Mach numbers well while at higher mach numbers the presence of large and irregular late time oscillations of the perturbation amplitude make it hard for the power law to fit as effectively. When the coefficients from the power law decay model are plotted versus Mach number, a distinct transition region can be seen. This region is likely to result from the transition of the post-shock SF_6 velocity from subsonic to supersonic range in the lab frame. This region separates the data into a high and low Mach number regions.

These regions each have their own correlation between the coefficients of the power law decay and the incident shock Mach number. At high Mach numbers, perturbations induced on the refracted shock wave will persist even at late times, and may act as a secondary source of baroclinic vorticity production in shock tube experiments after reshock. Therefore, one needs to be careful when pursuing reshock studies for the RMI at high Mach numbers. The end-wall should be far enough from the initial interface, which guarantees the planarity of the refracted shock wave before reaching the wall.

Further work remains to be done to explore the transition region experimentally and verify the results of the simulations presented here. Also, the strength of the refracted shock wave perturbations after reshock and their effect on the fluid interface should be explored further with experimental and simulation work.

Acknowledgments The authors would like to acknowledge the support of HEDP summer student program at LLNL, and to thank the scientists and staff that made this work possible. Also, we would like to thank, in particular, Mr. Cyrus Harrison for his data processing help and advice. This work was performed under the auspices of the US Department of Energy, Lawrence Livermore National Laboratory, under Contract No. DE-AC52-07NA27344. D.R. would also like to acknowledge the support of DOE-NNSA Grant No. DE-FG52-09NA29462.

References

1. Richtmyer, R.D.: Taylor instability in shock acceleration of compressible fluids. Commun. Pure Appl. Math. **13**, 297–319 (1960)
2. Meshkov, E.E.: Instability of the interface of two gases accelerated by a shock wave. Fluid Dyn. **4**, 101–104 (1972)
3. Brouillette, M.: The Richtmyer–Meshkov instability. Annu. Rev. Fluid Mech. **34**, 445–468 (2002)
4. Kane, J., Drake, R.P., Remington, B.A.: An evaluation of the Richtmyer–Meshkov instability in supernova remnant formation. Astrophys. J. **511**, 335–340 (1999)
5. Anderson, M.H., Puranik, B.P., Oakley, J.G., Brooks, P.W., Bonazza, R.: Shock tube investigation of hydrodynamic issues related to inertial confinement fusion. Shock Waves **10**, 377–387 (2000)
6. Zabusky, N.J.: Vortex paradigm for accelerated inhomogeneous flows: Visiometrics for the Rayleigh–Taylor and Richtmyer–Meshkov environments. Annu. Rev. Fluid Mech. **31**, 495–536 (1999)
7. Krivets, V.V., Long, C.C., Jacobs, J.W., Greenough, J.A.: Shock tube experiments and numerical simulation of the single mode three-dimensional Richtmyer-Meshkov instability. In: 26th International Symposium on Shock Waves. pp. 1205–1210. Springer, Gottingen (2009)
8. Motl, B., Oakley, J., Ranjan, D., Weber, C., Anderson, M., Bonazza, R.: Experimental validation of a Richtmyer–Meshkov scaling law over large density ratio and shock strength ranges. Phys. Fluids **21**, 126102 (2009)
9. Chapman, P.R., Jacobs, J.W.: Experiments on the three-dimensional incompressible Richtmyer–Meshkov instability. Phys. Fluids **18**, 074101 (2006)
10. Ranjan, D., Oakley, J., Bonazza, R.: Shock-bubble interactions. Annu. Rev. Fluid Mech. **43**, 117–140 (2011)
11. Ranjan, D., Niederhaus, J., Motl, B., Anderson, M., Oakley, J., Bonazza, R.: Experimental investigation of primary and secondary features in high-Mach-number shock-bubble interaction. Phys. Rev. Lett. **98**, 024502 (2007)
12. Ranjan, D., Anderson, M., Oakley, J., Bonazza, R.: Experimental investigation of a strongly shocked gas bubble. Phys. Rev. Lett. **94**, 184507 (2005)
13. Prestridge, K., Vorobieff, P., Rightley, P.M., Benjamin, R.F.: Validation of an instability growth model using particle image velocimetry measurements. Phys. Rev. Lett. **84**, 4353–4356 (2000)
14. Balakumar, B.J., Orlicz, G.C., Tomkins, C.D., Prestridge, K.P.: Particle-image velocimetry-planar laser-induced fluorescence measurements of Richtmyer–Meshkov instability growth in a gas curtain with and without reshock. Phys. Fluids **20**, 124103 (2008)
15. Brouillette, M., Sturtevant, B.: Experiments on the Richtmyer–Meshkov instability: small-scale perturbations on a plane interface. Phys. Fluids A Fluid **5**, 916–930 (1993)
16. Herrmann, M., Moin, P., Abarzhi, S.I.: Nonlinear evolution of the Richtmyer–Meshkov instability. J. Fluid Mech. **612**, 311–338 (2008)
17. Gupta, M.R., Roy, S., Khan, M., Pant, H.C., Sarkar, S., Srivastava, M.K.: Effect of compressibility on the Rayleigh–Taylor and Richtmyer–Meshkov instability induced nonlinear structure at two fluid interface. Phys. Plasmas **16**, 032303 (2009)
18. Rikanati, A., Oron, D., Sadot, O., Shvarts, D.: High initial amplitude and high Mach number effects on the evolution of the single-mode Richtmyer-Meshkov instability. Phys. Rev. E **67**, 026307 (2003)
19. Schilling, O., Latini, M.: High-order WENO simulations of three-dimensional reshocked Richtmyer-Meshkov instability to late times: dynamics, dependence on initial conditions, and comparisons to experimental data. Acta Math. Sci. **30**, 595–620 (2010)
20. Thornber, B., Drikakis, D., Youngs, D.L., Williams, R.J.R.: The influence of initial conditions on turbulent mixing due to Richtmyer–Meshkov instability. J. Fluid Mech. **654**, 99–139 (2010)
21. Leinov, E., Malamud, G., Elbaz, Y., Levin, L.A., Ben-Dor, G., Shvarts, D., Sadot, O.: Experimental and numerical investigation of the Richtmyer–Meshkov instability under re-shock conditions. J. Fluid Mech. **626**, 449–475 (2009)
22. Schilling, O., Latini, M., Don, W.: Physics of reshock and mixing in single-mode Richtmyer-Meshkov instability. Phys. Rev. E **76** (2007)
23. Niederhaus, J.H.J., Ranjan, D., Oakley, J.G., Anderson, M.H., Greenough, J.A., Bonazza, R.: Computations in 3D for shock-induced distortion of a light spherical gas inhomogeneity. In: Shock waves, Part XVIII. Springer, Berlin, pp 1169–1174. doi:10.1007/978-3-540-85181-3_60
24. Dimonte, G., Ramaprabhu, P.: Simulations and model of the nonlinear Richtmyer–Meshkov instability. Phys. Fluids **22**, 014104 (2010)
25. McFarland, J., Greenough, J., Ranjan, D.: Computational parametric study of a Richtmyer–Meshkov instability for an inclined interface. Phys. Rev. E **84**, 026303 (2011)
26. Aleshin, A.N., Zaitsev, S.G., Lazareva, E.V.: Damping of perturbations at a shock front in the presence of a Richtmyer–Meshkov instability. Sov. Tech. Phys. Lett. **17**, 493–496 (1991)
27. Aleshin, A.N., Chebotareve, E.I., Krivets, V.V., Lazareva, E.V., Sergeev, S.V., Titov, S.N., Zaytsev, S.: Investigation of Evolution of Interface After Its Interaction with Shock Waves. International Institute for Applied Physics and High Technology, Moscow (1996)
28. Kolev, T.V., Rieben, R.N.: A tensor artificial viscosity using a finite element approach. J. Comput. Phys. **228**, 8336–8366 (2009)
29. Sharp, R.W., Barton, R.T.: HEMP Advection Model. Lawrence Livermore Laboratory, Livermore (1981)